Chapter 3
Source Process of the 2011 Off the Pacific Coast of Tohoku Earthquake

Kimiyuki Asano, Haruko Sekiguchi, Tomotaka Iwata, Wataru Suzuki, Shin Aoi, and Takashi Kunugi

Abstract The kinematic source process of the 2011 Off the Pacific Coast of Tohoku earthquake is studied using strong motion data both in low- and high-frequency ranges. The slip distribution is estimated by the waveform inversion analysis using velocity waveforms in the frequency range from 0.01 to 0.125 Hz at strong motion stations along the Pacific coast. The strong motion generation area (SMGA) is estimated by the strong ground motion simulation in 0.1–10 Hz using the empirical Green's function method. The slip distribution is characterized by a large asperity with peak slip of 48 m which is imaged in the shallower portion of the source fault near the Japan Trench. Four SMGAs are identified in the deeper portion of the source fault. Unlike the past M7–8 subduction-zone plate-boundary events, the SMGAs and the asperity seem to be complementary in space. But the rupture time of each SMGA matches the timing of slip in each area. The total size of SMGAs is much smaller than the asperity area. This event coincides with empirical scaling relationships between total rupture area, asperity area, SMGA, and its seismic moment proposed for subduction-zone plate-boundary earthquakes by previous papers although the asperity abstracted for this event may have different nature from those of past smaller earthquakes.

Keywords Relationship between slip distribution and strong motion generation area • Scaling relationship • Source process of the 2011 Tohoku earthquake • Strong motion data • Strong motion generation area

K. Asano (✉) • H. Sekiguchi • T. Iwata
Disaster Prevention Research Institute (DPRI), Kyoto University, Uji, Japan
e-mail: k-asano@egmdpri01.dpri.kyoto-u.ac.jp

W. Suzuki • S. Aoi • T. Kunugi
National Research Institute for Earth Science and Disaster Prevention (NIED), Tsukuba, Japan

H. Kawase (ed.), *Studies on the 2011 Off the Pacific Coast of Tohoku Earthquake*,
Natural Disaster Science and Mitigation Engineering: DPRI reports,
DOI 10.1007/978-4-431-54418-0_3,

3.1 Introduction

The 2011 Off the Pacific Coast of Tohoku earthquake (Mw9.0, hereafter the 2011 Tohoku earthquake) which occurred at 14:46 on 11 March 2011 (JST = UT + 9) is the best observed megathrust earthquake, thanks to the present dense observation network in Japan. For example, nationwide dense strong motion observation networks K-NET and KiK-net operated by the National Research Institute for Earth Science and Disaster Prevention (NIED) (Aoi et al. 2004, 2011) succeeded in recording the acceleration waveforms during the mainshock at 1,223 stations as of December 2011 (Kunugi et al. 2012). The seismic intensity of 7 in the intensity scale of the Japan Meteorological Agency (JMA) was observed at Tsukidate, Kurihara city 175 km west of the epicentre, and the seismic intensity of 6+ was observed at many sites in Tohoku and Kanto districts (see, e.g. Hoshiba et al. 2011).

Figure 3.1 shows the spatial distribution of the observed peak ground acceleration (PGA) and the peak ground velocity (PGV) at strong motion stations in east and central Japan. These strong motion stations include the K-NET and KiK-net stations and the seismic intensity observation sites of JMA. Among these stations twenty stations in Tohoku and Kanto districts recorded ground accelerations larger than the gravitational acceleration.

Figure 3.2 shows the record sections of the north–south components of observed original acceleration waveforms and filtered velocity waveforms along the Pacific

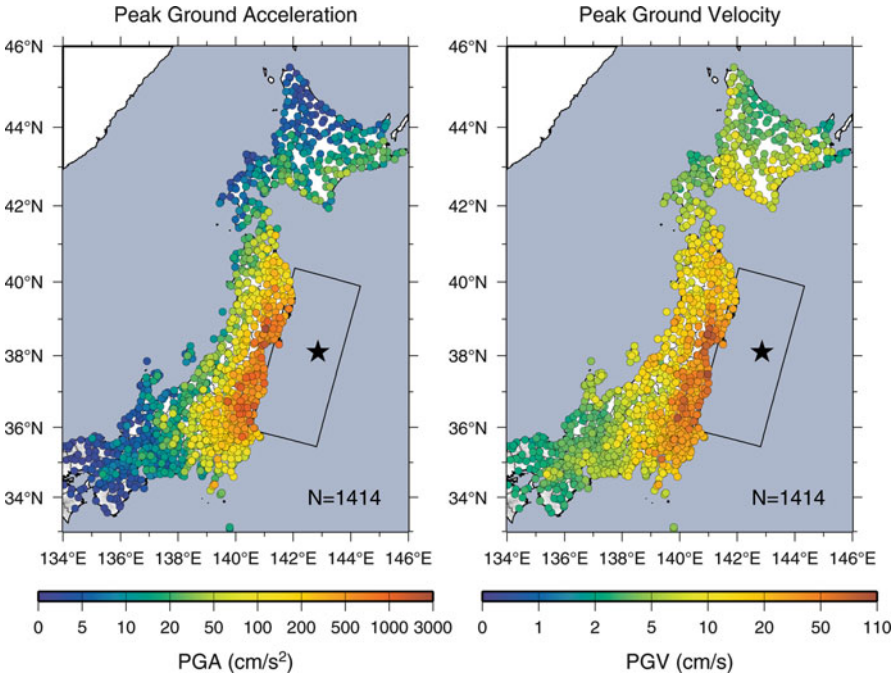

Fig. 3.1 Observed peak ground acceleration (*left*) and peak ground velocities (*right*) during the 2011 Tohoku earthquake at K-NET, KiK-net, and JMA strong motion stations

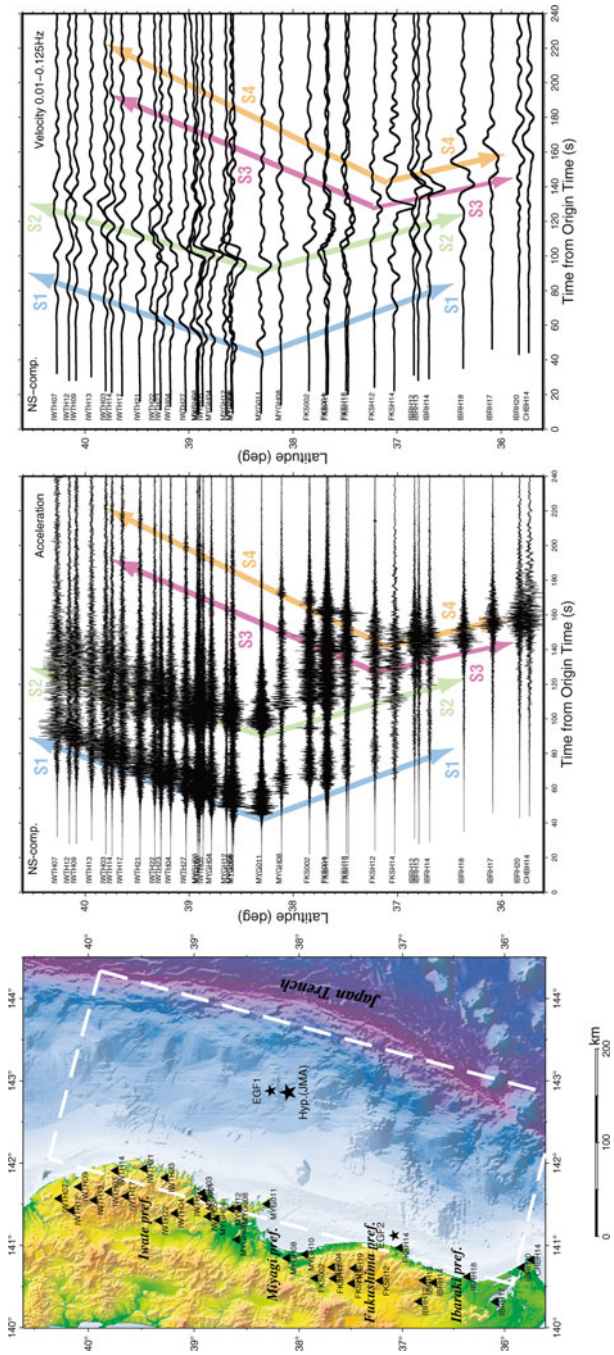

Fig. 3.2 Record sections of north–south components of observed original ground acceleration waveforms and filtered ground velocity waveforms in 0.01–0.125 Hz ordered by the latitude

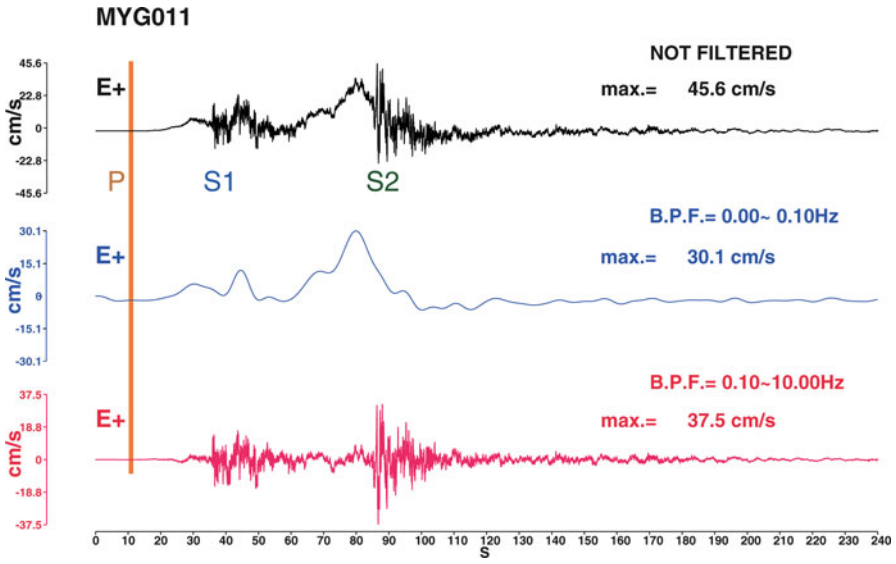

Fig. 3.3 Observed ground velocity waveforms of the east–west component at MYG011 without band-pass filter (*top*), low-pass filtered at 0.1 Hz (*middle*), and band-pass filtered between 0.1 and 10 Hz (*bottom*)

coast ordered by the latitude of stations. Four distinctive wave packets propagating northward and southward are recognized from the record section of the observed acceleration. Both the first (S1) and second wave packets (S2) are originated from off Miyagi prefecture, but S1 and S2 are separated by approximately 40 s. The third wave packet (S3) propagates from off Fukushima prefecture, and the fourth wave packet (S4) propagates from off the border between Fukushima and Ibaraki prefectures. Those observed characteristics of strong ground motions give us a brief image of the source process related to the strong ground motion generation during the 2011 Tohoku earthquake. However, these acceleration wave groups do not exactly correspond to the distinctive phases observed in the low-frequency (0.01–0.125 Hz) velocity waveforms, which means that spatiotemporal distributions of rupture contributing to high- and low-frequency wave radiation are different (Fig. 3.3).

In this chapter, we introduce the kinematic source process inverted from strong motion data in low-frequency band of 0.01–0.125 Hz by Suzuki et al. (2011) and the source model composed of strong motion generation areas (SMGAs) estimated by the forward modelling of broadband strong ground motion in 0.1–10 Hz by Asano and Iwata (2012). We will discuss the spatial relationship between large slip and SMGA to understand strong motion generation process during the 2011 Tohoku earthquake by comparing past subduction-zone plate-boundary earthquakes in northeast Japan.

3.2 Source Process by Waveform Inversion in Low-Frequency Band

3.2.1 Method

Suzuki et al. (2011) employed the multi-time-window linear waveform inversion method (Olson and Aspel 1982; Hartzell and Heaton 1983) to derive the rupture process. They assumed a rectangular fault model (Fig. 3.2), constructed to follow the geometry of the Pacific plate (Hasegawa et al. 1994). The strike and dip angles of the fault plane were set to 195° and 13°, respectively. The fault plane had a length of 510 km and a width of 210 km and was divided into 30×30 km^2 subfaults. The slip history of each subfault was represented by 25 6-s time windows, each of which was separated by 3 s, allowing slip for 78 s. The rupture starting point was set to 38.10°N, 142.85°E, 24 km deep, referring to the hypocentre determined by the NIED and JMA.

Strong motion data used for the inversion analysis was the S wave portion of the 0.01–0.125 Hz velocity waveforms of 10 K-NET stations and of 26 KiK-net borehole stations within 120–400 km epicentral distances. The observed and synthetic waveforms are aligned on the S wave arrivals. Green's functions were calculated using the discrete wave number method (Bouchon 1981) and the reflection/transmission matrix method (Kennett and Kerry 1979). The rupture propagation effect inside the subfault, expected from the first time window triggering velocity, was considered by convolving the moving dislocation (Sekiguchi et al. 2002). A one-dimensional underground structure model for the calculation of the Green's function was constructed for each station considering the three-dimensional crustal structure model (Fujiwara et al. 2009). The rupture process was inverted using the least squares method with an inequality constraint (Lawson and Hanson 1974), to limit the variation of the rake angle to within 90° centred at 90°, i.e. the pure dip slip angle. The smoothing constraint on slips was applied following the procedure proposed by Sekiguchi et al. (2000).

3.2.2 Result

Figure 3.4a, b shows the slip distribution estimated from their inversion analysis. The contour interval is 5 m. A large slip area, in which the slip is larger than 20 m, extends from the area around the hypocentre to the shallower part of the fault plane. A maximum slip of 48 m is estimated to the east of the hypocentre near the trench axis, far off Miyagi prefecture. The slips near the coastline are relatively small, except off Miyagi prefecture, where the slip is greater than 5 m from the coastline to the trench. The total seismic moment of the derived model is 4.42×10^{22} Nm (Mw9.0). The first time window triggering velocity of 3.2 km/s was selected because

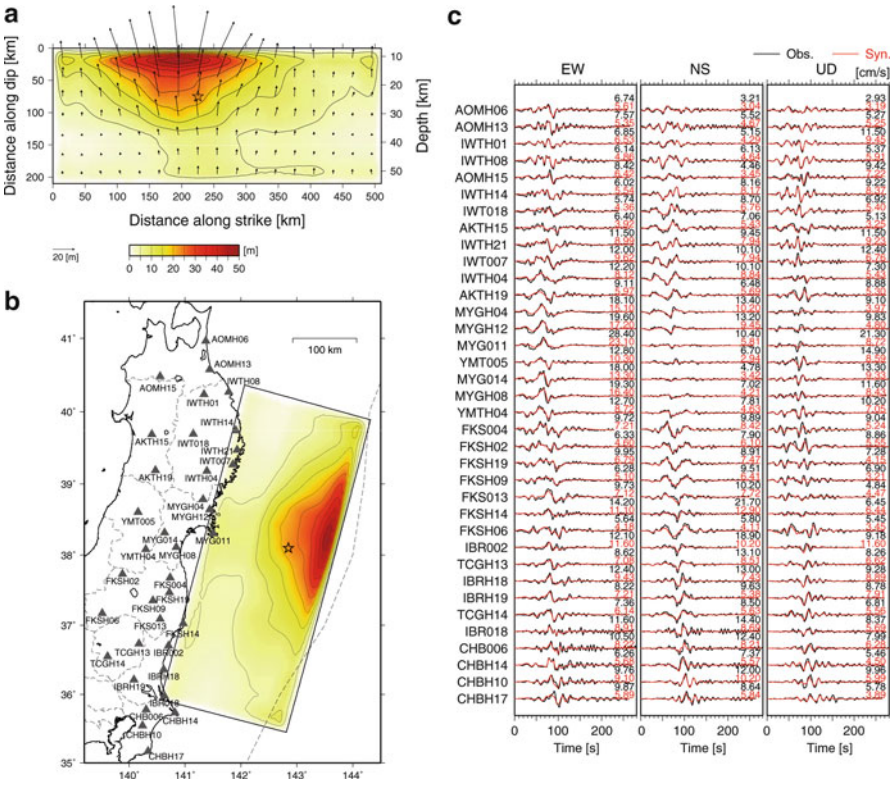

Fig. 3.4 **(a)** Slip distribution of the source fault plane, **(b)** slip distribution projected on the map, and **(c)** comparison between the observed (*black*) and synthetic (*red*) velocity waveforms between 0.01 and 0.125 Hz (Suzuki et al. 2011)

this velocity gives the smallest residual value (Fig. S1 in Suzuki et al. 2011). The observed and synthetic waveforms are compared in Fig. 3.4c. In order to observe the temporal characteristics, we show the slip distribution every 10 s with a contour interval of 1 m in Fig. 3.5. The first remarkable moment release started 20 s after the initial break, when the rupture occurred around the hypocentre. Then, at approximately 40 s, the rupture proceeded northward along the trench axis and toward the down-dip direction. Somewhat later, the rupture also extends southward along the trench axis. The largest slip event occurred from 60 to 100 s, with the rupture expanding toward the down-dip direction from the area along the trench axis. In this stage, large slip occurred continuously far offshore of southern Iwate, Miyagi, and northern Fukushima prefectures. The slip amount of the largest slip event was considerably decreased when raising the low-frequency limit of the data for the inversion to 0.02 Hz. This means that the largest slip event radiated seismic waves high in lower-frequency components (<0.02 Hz).

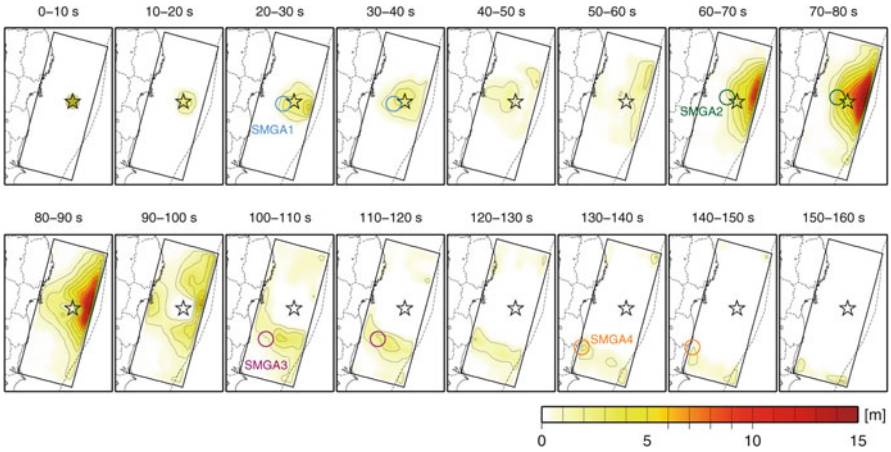

Fig. 3.5 Snapshot of slip amount at every 10 s from the initial break (Suzuki et al. 2011) with locations of SMGAs (Asano and Iwata 2012)

The last stage starts at around 100 s, where the rupture propagated southward in the area off Fukushima and Ibaraki prefectures. The entire rupture almost ceased within 150 s. The slip-velocity time function (Fig. 3 in Suzuki et al. 2011) shows that the subfaults around the hypocentre and the shallow part of the fault experienced two slip events.

3.3 SMGA Source Model for Strong Motion Simulation in 0.1–10 Hz

3.3.1 Location and Rupture Time of SMGAs

Asano and Iwata (2012) assumed that each wave packet S1–S4 seen in the record section of the observed acceleration waveforms (Fig. 3.2) is generated from corresponding strong motion generation area, SMGA1–SMGA4. SMGA is defined as the area characterized by a large uniform slip velocity within the total rupture area, which reproduce near-source strong ground motions up to about 10 Hz (Miyake et al. 2003). Asano and Iwata (2012) modelled those SMGAs to fit the simulated ground motions to the observed ones. They fixed the hypocentre at the location determined routinely by JMA (red star in Fig. 3.6) and assumed that each SMGA is on the surface of the subducting Pacific slab, whose depth was determined by Nakajima and Hasegawa (2006) and Nakajima et al. (2009).

Asano and Iwata (2012) read the onset of S1–S4 in the observed waveforms at K-NET and KiK-net stations along the coast to determine the location of rupture

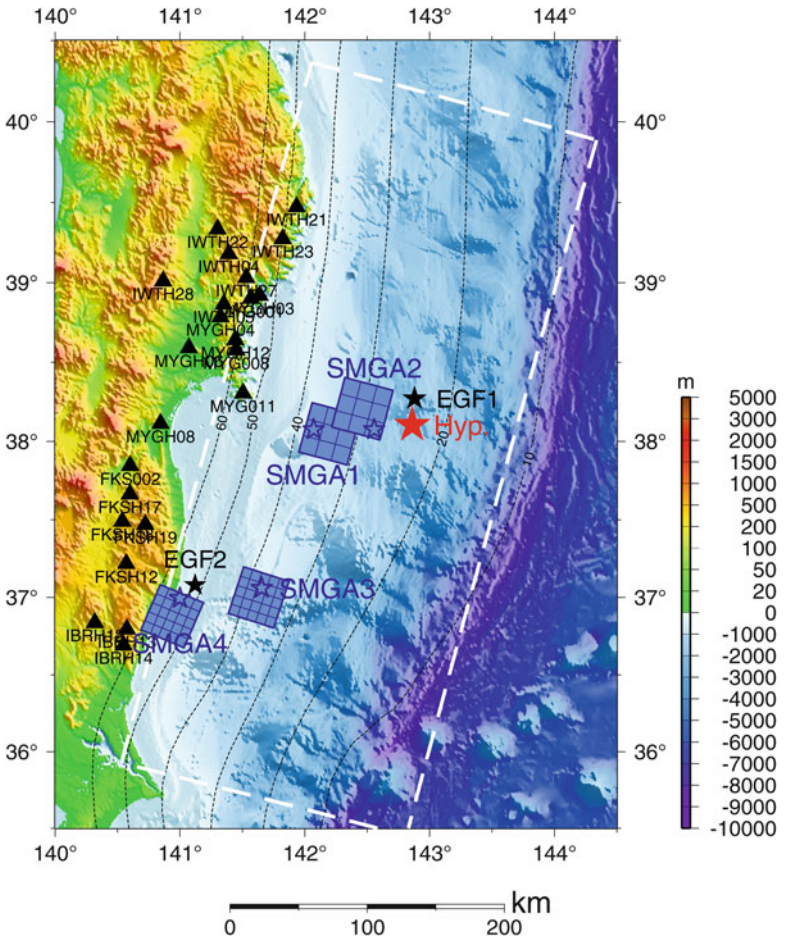

Fig. 3.6 Source model for broadband strong motion simulation between 0.1 and 10 Hz composed of four SMGAs projected on the map (Asano and Iwata 2012)

starting point and rupture time for each SMGA objectively. The optimum set of parameters was determined to minimize the root mean square of difference between the observed and theoretical travel times by grid search. The one-dimensional velocity structure model was assumed, and the difference between the observed and theoretical travel times was corrected by using an Mw6.0 foreshock (EGF1 in Fig. 3.6) occurring at 03:16 on 10 March 2011 (JST) as a reference event, whose location was fixed at the hypocentre determined by JMA. The search intervals in the grid search were 0.005° for latitude and longitude and 0.1 s for rupture time.

The estimated locations of the rupture starting points of the four SMGAs are indicated by the open stars in Fig. 3.6. The rupture delay times from the origin time are estimated to be 24.1, 65.4, 106.5, and 133.0 s, respectively. The spatial

uncertainty in the dip direction is relatively larger than that in the strike direction due to the nonuniform distribution of observed stations surrounding the source region (see Asano and Iwata 2012).

3.3.2 SMGA Source Modelling for Broadband Strong Ground Motion Simulation

Asano and Iwata (2012) constructed the source model composed of four SMGAs based on broadband strong motion simulation from 0.1 to 10 Hz using the empirical Green's function method by Irikura (1986). In this method, the ground motion for a target event is synthesized by summing up the records of small events with a filtering function which corrects the difference in the slip-velocity time function between the large and small events following the source scaling law and the ω^{-2} source spectral model (Irikura 1986; Miyake et al. 2003). These scaling relationships are controlled by two parameters N, which corresponds to the ratio of spatial dimension and slip amount between the large and small events, and C, which corrects the difference in the stress drop between the large and small events.

The scaling parameters N and C were determined for each SMGA by a source spectral fitting method (Miyake et al. 1999, 2003). This method derives these parameters by fitting the observed source spectral ratio between the large and small events to the theoretical source spectral ratio following the ω^{-2} source spectral model. The moment ratio and the corner frequency of the target and small events were estimated by the grid search algorithm. The propagation path effects were corrected for geometrical spreading for the body waves and an attenuation factor. The frequency-dependent quality factor, $Q(f) = 110f^{0.69}$ obtained by Satoh et al. (1997) in this region and the S wave velocity of 4.46 km/s were used to correct the attenuation factor. The records of an Mw6.0 event, which occurred at 03:16 on 10 March 2011 (JST), were used as EGF for SMGA1 and SMGA2 (EGF1), and those of an Mw5.5 event, which occurred at 22:12 on 22 October 2005 (JST), were used as EGF for SMGA3 and SMGA4 (EGF2). The epicentres of two EGF events are shown in Fig. 3.6. N values are 3, 3, 5, and 5 for SMGA1, SMGA2, SMGA3, and SMGA4, respectively. C values were estimated to be 10.6 and 4.0 for SMGA3 and SMGA4, respectively. C values for SMGA1 and SMGA2 were searched together with other unknown parameters in the following strong motion simulations because these C values were not constrained well by the source spectral fitting method due to the small number of N.

Then, the source parameters of the four SMGAs were estimated based on the broadband strong motion simulations using the empirical Green's function method. The best set of parameters was searched by minimizing the residuals of acceleration envelopes and displacement waveforms through a grid search (Miyake et al. 1999, 2003). The parameters to be estimated by the grid search are the spatial dimensions, rise times of the EGF events, the stress drops (i.e. C values) and rupture starting subfaults of each SMGA, and the rupture propagation velocities within the SMGAs. The length L, width W, and rise time T of the SMGA are given by Nl, Nw, $N\tau$ from

Table 3.1 Source parameters of SMGAs

	SMGA1	SMGA2	SMGA3	SMGA4
Latitude (°N)	38.075	38.075	37.060	36.995
Longitude (°E)	142.070	142.555	141.655	141.000
Depth (km)	36.8	28.0	37.1	53.8
Rupture time (s)	24.1	65.4	106.5	133.0
Strike (°)	195	195	198	203
Dip (°)	13	13	17	20
N	3	3	5	5
C	12.0	14.0	10.6	4.0
Length (km)	36	36	35	35
Width (km)	36	36	35	35
Area (km^2)	1,296	1,296	1,225	1,225
Rise time (s)	6.90	6.90	1.70	1.70
Seismic moment (Nm)	4.57×10^{20}	5.33×10^{20}	3.07×10^{20}	1.16×10^{20}
Stress drop (MPa)	23.9	27.8	17.5	6.6
Slip amount (m)	5.2	6.1	3.7	1.4

Latitude, longitude, and depth are defined at the rupture starting point of individual SMGA

the length l, width w, and rise time τ of the EGF event. The search range and its grid interval of the model parameters in the grid search are referred to Asano and Iwata (2012). The stress drops of the EGF events were calculated assuming the circular crack source model (Eshelby 1957). The strike and dip angles of each SMGA were determined based on the local geometry of the plate interface (Nakajima and Hasegawa 2006; Nakajima et al. 2009). The deeper SMGA has slightly steeper dip angle because of the bending of the subducting Pacific slab. The strong motion stations used in this modelling are indicated by the solid triangles in Fig. 3.6.

3.3.3 Result

Figure 3.6 shows a map view of the estimated source model. The source parameters of each SMGA are listed in Table 3.1. The rupture within SMGA1 propagates towards the up-dip direction, whereas that within SMGA2 propagates towards the down-dip directions. The ruptures of SMGA3 and SMGA4 located southwest of the hypocentre mainly propagate in southwest direction. The rupture propagation velocity within each SMGA is 4.0 km/s. The stress drops of four SMGAs range from 6.6 to 27.8 MPa.

Figure 3.7 shows the comparison between the observed and synthetic acceleration, velocity, and displacement waveforms in the frequency range from 0.1 to 10 Hz at 23 strong motion stations. The synthetic ground motions explain well the characteristics of observed ground motion in the broadband frequency range.

Asano and Iwata (2012) pointed out that SMGA1, SMGA2, and SMGA3 spatially overlap the source area of past M7 class earthquakes in 1936, 1933, and 1938, respectively.

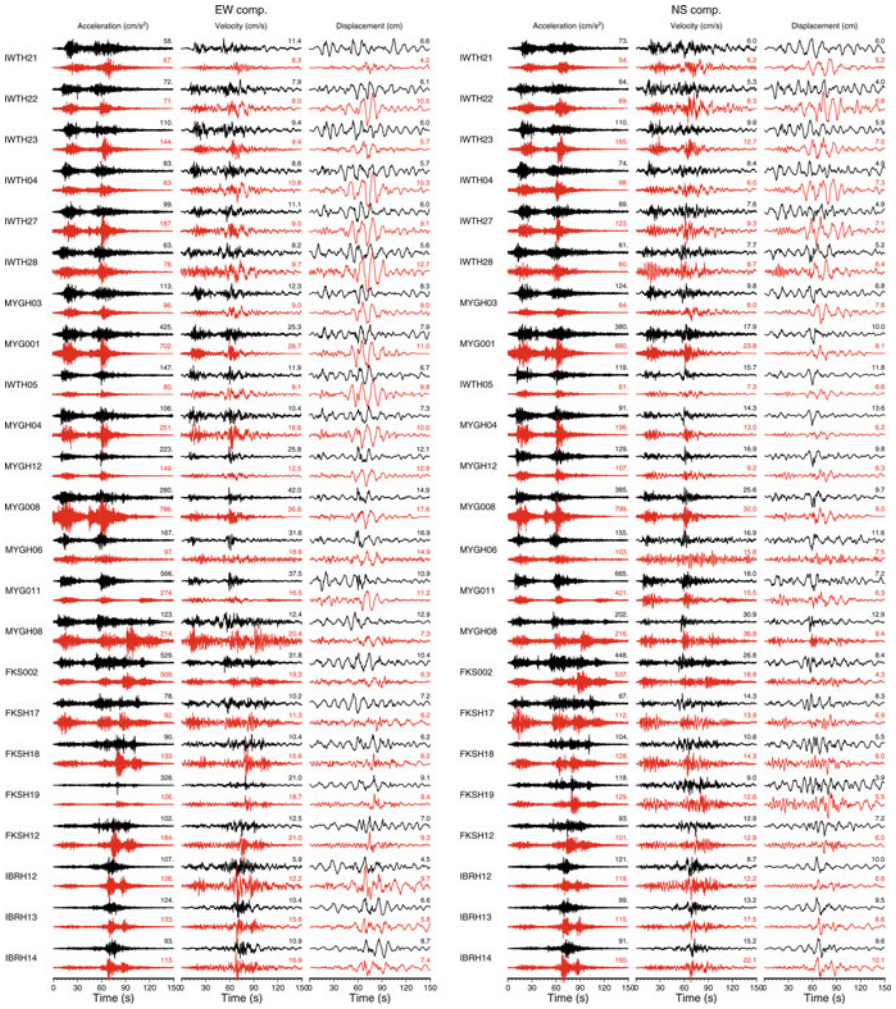

Fig. 3.7 Comparison between the observed and synthetic horizontal acceleration, velocity, and displacement waveforms in 0.1–10 Hz (Asano and Iwata 2012)

3.4 Relationship Between Heterogeneous Rupture Process and Strong Motion Generation Areas

3.4.1 Spatial Relationship Between Slip Distribution and SMGAs

The spatial relationship between large slip area and SMGA has been argued for past earthquakes. As for inland crustal earthquakes, Miyake et al. (2003) concluded that the location and size of SMGA correspond to the asperity, or large slip area on the

source fault. Suzuki and Iwata (2007) analysed the 2005 off Miyagi earthquake (M_{JMA} 7.2), which was a subduction-zone plate-boundary event occurring west of the epicentre of the 2011 Tohoku earthquake. They confirmed that two SMGAs of the 2005 off Miyagi earthquake existed inside the asperity area estimated by the kinematic waveform inversions but size of that area was significantly smaller than asperity area. The source model of the 2003 off Tokachi earthquake (M_{JMA} 8.0) also shows the same features (Kamae and Kawabe 2004). That is, most cases of past subduction-zone plate-boundary earthquakes show the overlap of asperity and SMGA areas. It should be noted that the kinematic waveform inversion studies for the 2003 off Tokachi and 2005 off Miyagi earthquakes use finer spatial grid than current studies for the 2011 Tohoku earthquake and the analysed frequency range is partly overlapped with those used for SMGA modelling. Suzuki (2008) proposed a hierarchical broadband source model for plate-boundary earthquake in which SMGA is a localized area inside the asperity area having particularly high slip velocity.

The SMGAs of the 2011 Tohoku earthquake by Asano and Iwata (2012) and the final slip distribution obtained by Suzuki et al. (2011) are compared in Fig. 3.8. SMGA2 is located near the edge of the asperity and the others are outside the asperity. That is, the large slip area and SMGAs are apparently not overlapped in space for the 2011 Tohoku earthquake. It is a significant characteristic of this event that is different from past M7–8 subduction-zone plate-boundary events in this region. The frequency dependence of rupture process is one answer for the question why SMGA and asperity is apparently complementary in space. Recently, Lay et al. (2012) proposed depth-varying seismic characteristics with four distinct failure domains (domain A to D) extending along the megathrust from the trench to the down-dip edge of the seismogenic zone based on the analyses for three megathrust earthquakes in the world. The domain B from 15 to 35 km deep, which is defined as a portion generating large displacements over large-scale region with only modest coherent high-frequency radiation, corresponds to the asperity of this event. The domain C from 35 to 55 km deep defined as rupture of smaller isolated patches producing bursts of coherent high-frequency energy corresponds to four SMGAs.

In order to see temporal relationship between slip progression and SMGA rupture, the locations of the four SMGA estimated by Asano and Iwata (2012) are compared with the temporal slip history in low-frequency range estimated by Suzuki et al. (2011) in Fig. 3.5. The rupture time of the four SMGAs matches the timing of slip occurrence in each area on the fault plane. This figure implies the possibility that smaller scale local slip peaks in the inverted source process match the SMGAs and such local slip peaks are masked by the dominating large slip near the trench in the final slip distribution.

For solving this problem, the more detailed slip inversion analysis using higher-frequency waveforms, finer spatial grids, and reliable Green's functions is required to see whether the localized small asperity or high slip-velocity area corresponding to SMGAs can be resolved or not.

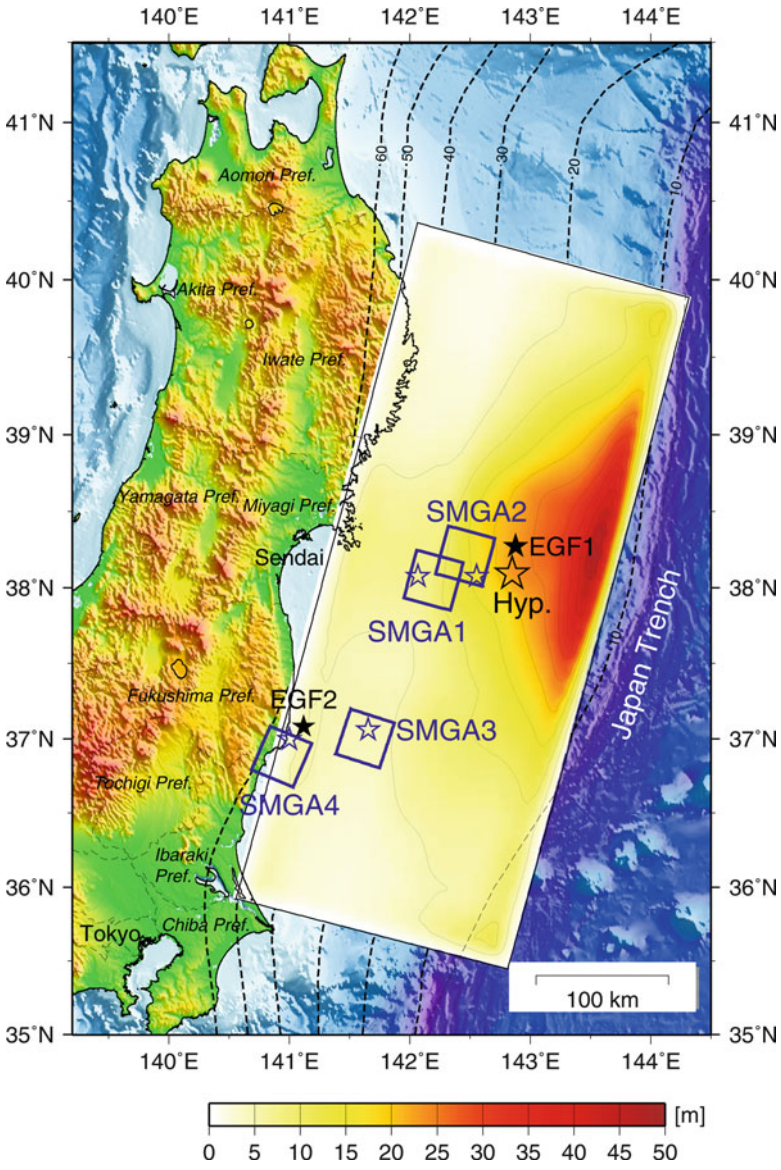

Fig. 3.8 Spatial comparison between SMGAs by Asano and Iwata (2012) and final slip distribution by Suzuki et al. (2011)

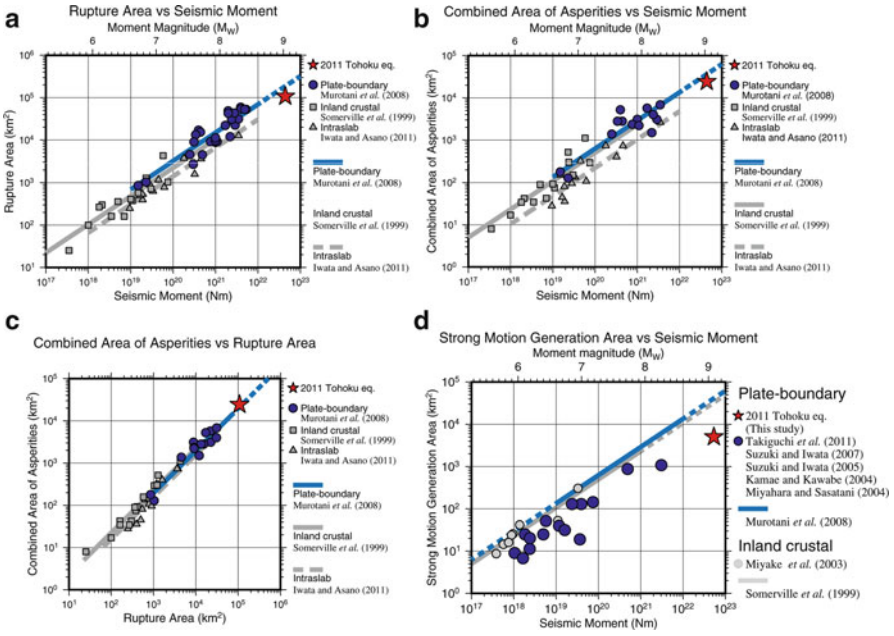

Fig. 3.9 Scaling relationships between **(a)** total rupture area and seismic moment, **(b)** combined area of asperities and seismic moment, **(c)** combined area of asperities and total rupture area, and **(d)** strong motion generation area and seismic moment

3.4.2 Scaling Relationships

In this section, we compare the source features of this earthquake obtained by Asano and Iwata (2012) and Suzuki et al. (2011) with the empirical scaling relationships between the size of SMGA and seismic moment and between rupture area and asperity area.

The empirical scaling relationships between rupture area, total asperity area, and seismic moment for plate-boundary earthquakes are studied by Murotani et al. (2008). Murotani et al. (2008) compiled the heterogeneous slip models of 26 plate-boundary earthquakes in Japan and characterized the total rupture area and asperities following the procedure proposed by Somerville et al. (1999). We extracted the total rupture area and asperities of the 2011 Tohoku earthquake following the same procedure and found them as 107,100 and 24,300 km^2, respectively. Those values are plotted in Fig. 3.9a–c together with other events studied in the previous studies. The rupture area and asperity of the 2011 Tohoku earthquake follow the empirical scaling relationship by Murotani et al. (2008). The rupture area and asperity of plate-boundary earthquakes have relatively larger dimensions than those of inland crustal (Somerville et al. 1999) and intraslab earthquakes (Iwata and Asano 2011) of the same seismic moment. But we have to be careful in treating the asperity area abstracted for this earthquake by the conventional method. As discussed in the

Subsection 3.4.1, the asperity of this event radiated low-frequency dominantly and does not include SMGAs. Its nature may be different from those abstracted for the past M7–8 plate-boundary earthquakes.

Combined area of SMGAs of the 2011 Tohoku earthquake obtained by Asano and Iwata (2012) is 5,042 km^2. The total size of SMGA is about 1/5 of the asperity area. This value against the seismic moment is plotted in Fig. 3.9d together with the SMGA areas for the other earthquakes. SMGA source models have been constructed for past plate-boundary earthquakes in northeast Japan: the 1994 far off Sanriku earthquake (Mw7.7) by Miyahara and Sasatani (2004), the 2003 off Tokachi earthquake (Mw8.3) by Kamae and Kawabe (2004), the 2005 off Miyagi earthquake (Mw7.2) by Suzuki and Iwata (2007), and the 1982 and 2008 off Ibaraki earthquakes (Mw7.0 and 6.8) by Takiguchi et al. (2011). Suzuki and Iwata (2005) analysed other Mw6.0–7.0 plate-boundary earthquakes in northeast Japan. Miyake et al. (2003) analysed SMGA for inland crustal events in Japan and concluded that the size of SMGA corresponds to the size of asperity for inland crustal earthquakes. That is, SMGA for inland crustal earthquakes follows the empirical scaling relationship for asperity and seismic moment proposed by Somerville et al. (1999). On the other hand, the size of SMGA of plate-boundary earthquakes in northeast Japan is smaller than those of inland crustal earthquakes of the same seismic moment. This fact indicates that the stress drop of SMGA for subduction-zone plate-boundary earthquakes is larger than that of inland crustal earthquakes (Suzuki and Iwata 2007). The 2011 Tohoku earthquake also shows similar tendency with previous subduction-zone plate-boundary earthquakes.

3.5 Source Models by Other Research Groups

For the 2011 Tohoku earthquake, many research groups in seismology and geodesy are extensively working on analysing the heterogeneous source process using various kinds of data (strong motion, teleseismic body and surface waves, static and high-rate GPS, InSAR, tsunami waveform, etc.). In Table 3.2, we summarize the spatiotemporal heterogeneous slip models derived using seismological data (e.g. strong motion, teleseismic, and high-rate GPS data) from published papers. Most of papers use multiple time windows for each subfault in their source inversion analysis (Ide et al. 2011; Koketsu et al. 2011; Lay et al. 2011; Lee et al. 2011; Suzuki et al. 2011; Yagi and Fukahata 2011a; Yokota et al 2011; Yoshida et al. 2011a, b; Yue and Lay 2011), whereas the others use single time window with variable slip duration (Ammon et al. 2011; Hayes 2011; Shao et al. 2011). Peak slip amount in these source models varies from 28 to 63 m. The rupture dimension differs by a factor of two.

SMGA source model is also published by Kurahashi and Irikura (2011). Back-projection analyses using teleseismic and regional array dataset are studied to infer frequency-dependent seismic wave radiation process on the fault (Honda et al. 2011; Ishii 2011; Kiser and Ishii 2012; Koper et al. 2011; Meng et al. 2011; Roten et al. 2012; Wang and Mori 2011; Zhang et al. 2011).

Table 3.2 Summary of source models using seismological data

Reference	Data	Hypocentre information	Strike/dip	Fault size (km^2)	Subfault size (km^2)	Vr (km/s)	Seismic moment (Nm)	Peak slip (m)	Inversion method
Ammon et al. (2011)	Teleseismic P and Rayleigh High-rate GPS	USGS	202/12	600×210	15×15	1.5 ($r<100$ km), 2.5	3.64×10^{22}	41	Ammon et al. (2005)
Hayes (2011)	Teleseismic P&SH (0.005–1 Hz) Rayleigh and Love (0.002–0.005 Hz)	USGS	194/10	625×260	25×20	Variable	4.90×10^{22}	33	Ji et al. (2002)
Ide et al. (2011)	Teleseismic P (0.005–1 Hz)	–	–	440×240	20×20	Infinity	4.5×10^{22}	30	Ide (2001)
Koketsu et al. (2011)	Teleseismic P (0.002–0.25 Hz) Strong motion (0.01–0.1 Hz) GPS static disp	JMA + dep. 17 km	200/12	480×150	30×30	2.5	3.8×10^{22}	36	Yoshida et al. (1996)
Lay et al. (2011)	Teleseismic P	Zhao et al. (2011)	202/10	380×200	20×20	1.5 ($r<100$ km), 2.5	4.0×10^{22}	63	Kikuchi and Kanamori (2003)
Lee et al. (2011)	Teleseismic P (0.005–0.2 Hz) Strong motion (0.01–0.2 Hz) GPS static disp.	JMA	193/14	660×240	20×20	3.5	3.67×10^{22}	50	Lee et al. (2006)
Shao et al. (2011)	Teleseismic P&SH (0.003–0.5 Hz) Rayleigh and Love (0.003–0.006 Hz)	JMA	198/10	475×200	25×20	Variable	5.75×10^{22}	59	Ji et al. (2002)
Suzuki et al. (2011)	Strong motion (0.01–0.125 Hz)	NIED and JMA	195/13	510×210	30×30	3.2	4.42×10^{22}	48	Hartzell and Heaton (1983)
Yagi and Fukahata (2011a)	Teleseismic P (0.001–0.38 Hz)	JMA + dep. 22 km	200/12	500×200	20×20	2.8	5.7×10^{22}	51	Yagi and Fukahata (2011b)
Yokota et al. (2011)	Teleseismic P (0.002–0.25 Hz) Strong motion (0.01–0.1 Hz) GPS static disp. tsunami	JMA + dep. 17 km	200/5, 12, 20	480×180	30×30	2.5	4.2×10^{22}	35	Yoshida et al. (1996)
Yoshida et al. (2011a)	Strong motion (0.005–0.05 Hz)	JMA	193/10	468×228	12×12	2.5	4.3×10^{22}	47	Hartzell and Heaton (1983)
Yoshida et al. (2011b)	Teleseismic P (0.002–1 Hz)	JMA	201/9	510×240	30×30	1.8	4.3×10^{22}	28	Kikuchi and Kanamori (2003)
Yoshida et al. (2011b)	Strong motion (0.01–0.15 Hz)	JMA	201/9	475×175	25×25	2.5	3.4×10^{22}	38	Ide et al. (1996)
Yue and Lay (2011)	High-rate GPS (DC-0.04 Hz)	Zhao et al. (2011)	202/10, 22	475×175	20×20	1.5 ($r<100$ km), 2.5	4.8×10^{22}	60	Hartzell and Heaton (1983)

3.6 Summary

We compared the source process of the 2011 Tohoku earthquake seen in lower- and higher-frequency bands and discussed their relation based on the kinematic source model inverted from strong motion data in 0.01–0.125 Hz by Suzuki et al. (2011) and the SMGA model estimated by the forward modelling of strong ground motion in 0.1–10 Hz by Asano and Iwata (2012). The slip distribution is characterized by a large asperity with peak slip of 48 m which is imaged in the shallower portion of the source fault near the Japan Trench east of the epicentre rupturing from 60 to 100 s after the initial break. The entire rupture lasted about 150 s. Four SMGAs are identified in the deeper portion of the source fault. The rupture area and asperity of the 2011 Tohoku earthquake coincide with the empirical scaling relationship for plate-boundary earthquake derived by Murotani et al. (2008). Although the asperity of this event abstracted based on slip amount may have different nature from those of past earthquakes compiled in Murotani et al. (2008), the SMGA area is significantly smaller than asperity area, which is similar to past plate-boundary events in north-east Japan. Unlike past events, the SMGAs and the asperity apparently do not overlap for this earthquake, whereas the rupture time of each SMGA matches the timing of slip in each area. This is a significant difference between the 2011 Tohoku earthquake and past M7–8 subduction-zone plate-boundary events in this region. The frequency-dependent characteristics of spatiotemporal slip history of this event might cause this difference because the target frequency ranges of current two studies almost do not overlap. The source modelling for strong motion prediction of future subduction-zone plate-boundary mega earthquakes should be advanced based on the knowledge obtained from this event.

Acknowledgments The strong motion data of K-NET, KiK-net, and JMA are used in this study. The digital data of the geometry of the Pacific plate is compiled and provided via the Internet by Dr. Fuyuki Hirose at the Meteorological Research Institute of JMA. Most of figures were produced by using the Generic Mapping Tools (Wessel and Smith 1998).

References

Ammon CJ, Ji C, Thio H-K, Robinson D, Ni S, Hjorleifsdottir V, Kanamori H, Lay T, Das S, Helmberger DV, Ichinose G, Polet J, Wald D (2005) Rupture process of the great 2004 Sumatra-Andaman earthquake. Science 308(5725):1133–1139

Ammon CJ, Lay T, Kanamori H, Cleveland M (2011) A rupture model of the 2011 off the Pacific coast of Tohoku earthquake. Earth Planets Space 63(7):693–696

Aoi S, Kunugi T, Fujiwara H (2004) Strong-motion seismograph network operated by NIED: K-NET and KiK-net. J Jpn Assoc Earthq Eng 4(3):65–74

Aoi S, Kunugi T, Nakamura H, Fujiwara H (2011) Deployment of new strong motion seismographs of K-NET and KiK-net. In: Akkar S et al (eds) Earthquake data in engineering seismology. Geotechnical, Geological and Earthquake Engineering 14. Springer, Dordrecht, pp 167–186

Asano K, Iwata T (2012) Source model for strong ground motion in 0.1–10 Hz during the 2011 Tohoku earthquake. Earth Planets Space 64(12):1111–1123

Bouchon M (1981) A simple method to calculate Green's function for elastic layered media. Bull Seismol Soc Am 71(4):959–971
Eshelby JD (1957) The determination of the elastic field of an ellipsoidal inclusion, and related problems. Proc Roy Soc A 241(1226):376–396
Fujiwara H, Kawai S, Aoi S, Morikawa N, Senna S, Kudo N, Ooi M, Hao K, Hayakawa Y, Toyama N, Matsuyama H, Iwamoto K, Suzuki H, Liu Y (2009) A study on subsurface structure model for deep sedimentary layers of Japan for strong-motion evaluation. Technical Note of the NIED 337, DVD-ROM (in Japanese)
Hartzell SH, Heaton TH (1983) Inversion of strong ground motion and teleseismic waveform data for the fault rupture history of the 1979 Imperial Valley, California, earthquake. Bull Seismol Soc Am 73(6A):1553–1583
Hasegawa A, Horiuchi S, Umino N (1994) Seismic structure of the northeastern Japan convergent margin: a synthesis. J Geophys Res 99(11):22,295–22,311
Hayes GP (2011) Rapid source characterization of the 2011 Mw9.0 off the Pacific coast of Tohoku earthquake. Earth Planets Space 63(7):529–534
Honda R, Yukutake Y, Ito H, Harada M, Aketagawa T, Yoshida A, Sakai S, Nakagawa S, Hirata N, Obara K, Kimura H (2011) A complex rupture image of the 2011 off the Pacific coast of Tohoku Earthquake revealed by the MeSO-net. Earth Planets Space 63(7):583–588
Hoshiba M, Iwakiri K, Hayashimoto N, Shimoyama T, Hirano K, Yamaya Y, Ishigaki Y, Kikuta H (2011) Outline of the 2011 off the Pacific coast of Tohoku Earthquake. Earth Planets Space 63(7):547–551
Ide S (2001) Complex source processes and the interaction of moderate earthquakes during the earthquake swarm in the Hida-Mountains, Japan, 1998. Tectonophysics 334(1):35–54
Ide S, Takeo M, Yoshida Y (1996) Source process of the 1995 Kobe earthquake: determination of spatio-temporal slip distribution by Bayesian modeling. Bull Seismol Soc Am 86(3):547–566
Ide S, Baltay A, Beroza GC (2011) Shallow dynamic overshoot and energetic deep rupture in the 2011 Mw9.0 Tohoku-Oki earthquake. Science 332(6036):1426–1429
Irikura K (1986) Prediction of strong acceleration motions using empirical Green's function. In: Proceedings of the 7th Japan earthquake engineering symposium, Tokyo, pp 151–156
Ishii M (2011) High-frequency rupture properties of the Mw9.0 off the Pacific coast of Tohoku earthquake. Earth Planets Space 63(7):609–614
Iwata T, Asano K (2011) Characterization of the heterogeneous source model of intraslab earthquakes toward strong ground motion prediction. Pure Appl Geophys 168(1–2):117–124
Ji C, Wald D, Helmberger DV (2002) Source description of the 1999 Hector Mine, California, earthquake, part I: Wavelet domain inversion theory and resolution analysis. Bull Seismol Soc Am 92(4):1192–1207
Kamae K, Kawabe H (2004) Source model composed of asperities for the 2003 Tokachi-oki, Japan, earthquake (M_{JMA}=8.0) estimated by the empirical Green's function method. Earth Planets Space 56(3):323–327
Kennett BLN, Kerry NJ (1979) Seismic waves in a stratified half space. Geophys J Roy Astr Soc 57(3):557–583
Kikuchi M, Kanamori H (2003) Note on teleseismic body-wave inversion program. http://www.eri.u-tokyo.ac.jp/ETAL/KIKUCHI/
Kiser E, Ishii M (2012) The March 11, 2011 Tohoku-oki earthquake and cascading failure of the plate interface. Geophys Res Lett 39:L00G25. doi:10.1029/2012GL051170
Koketsu K, Yokota Y, Nishimura N, Yagi Y, Miyazaki S, Satake K, Fujii Y, Miyake H, Sakai S, Yamanaka Y, Okada T (2011) A unified source model for the 2011 Tohoku earthquake. Earth Planet Sci Lett 310(3–4):480–487
Koper KD, Hutko AR, Lay T, Ammon CJ, Kanamori H (2011) Frequency-dependent rupture process of the 2011 Mw9.0 Tohoku earthquake: comparison of short-period P wave backprojection images and broadband seismic rupture models. Earth Planets Space 63(7):599–602
Kunugi T, Aoi S, Suzuki W, Nakamura H, Morikawa N, Fujiwara H (2012) Strong motions of the 2011 Tohoku-Oki earthquake. Natural Disaster Research Report, NIED 48:63–72 (in Japanese with English abstract)

Kurahashi S, Irikura K (2011) Source model for generating strong ground motions during the 2011 off Pacific coast of Tohoku earthquake. Earth Planets Space 63(7):571–576

Lawson CL, Hanson RJ (1974) Solving least squares problems. Prentice-Hall, New Jersey, 340 pp

Lay T, Ammon CJ, Kanamori H, Xue L, Kim MJ (2011) Possible large near-trench slip during the 2011 Mw9.0 off the Pacific coast of Tohoku earthquake. Earth Planets Space 63(7): 687–692

Lay T, Kanamori H, Ammon CJ, Koper KD, Hutko AR, Ye L, Yue H, Rushing TM (2012) Depth-varying rupture properties of subduction zone megathrust earthquakes. J Geophys Res 117(B4):B04311. doi:10.1029/2011JB009133

Lee S-J, Ma K-F, Chen H-W (2006) Three-dimensional dense strong motion waveform inversion for the rupture process of the 1999 Chi-Chi, Taiwan, earthquake. J Geophys Res 111(B11):B11308. doi:10.1029/2005JB004097

Lee S-J, Huang B-S, Ando M, Chiu H-C, Wang J-H (2011) Evidence of large scale repeating slip during the 2011 Tohoku-Oki earthquake. Geophys Res Lett 38(19):L19306. doi:10.1029/2011GL049580

Meng L, Inbal A, Ampuero J-P (2011) A window into the complexity of the dynamic rupture of the 2011 Mw9 Tohoku-Oki earthquake. Geophys Res Lett 38:L00G07. doi:10.1029/2011GL048118

Miyahara S, Sasatani T (2004) Estimation of source process of the 1994 Sanriku Haruka-oki earthquake using empirical Green's function method. Geophys Bull Hokkaido Univ 67:197–212 (in Japanese with English abstract)

Miyake H, Iwata T, Irikura K (1999) Strong ground motion simulation and source modeling of the Kagoshima-ken Hokuseibu earthquakes of March 26 (M_{JMA} 6.5) and May 13 (M_{JMA} 6.3), 1997, using empirical Green's function method. Zisin 2 (J Seism Soc Jpn) 51(4):431–442 (in Japanese with English abstract)

Miyake H, Iwata T, Irikura K (2003) Source characterization for broadband ground-motion simulation: kinematic heterogeneous source model and strong motion generation area. Bull Seismol Soc Am 93(6):2531–2545

Murotani S, Miyake H, Koketsu K (2008) Scaling of characterized slip models for plate-boundary earthquakes. Earth Planets Space 60(9):987–991

Nakajima J, Hasegawa A (2006) Anomalous low-velocity zone and linear alignment of seismicity along it in the subducted Pacific slab beneath Kanto, Japan: reactivation of subducted fracture zone? Geophys Res Lett 33(16):L16309. doi:10.1029/2006GL026773

Nakajima J, Hirose F, Hasegawa A (2009) Seismotectonics beneath the Tokyo metropolitan area, Japan: effect of slab-slab contact and overlap on seismicity. J Geophys Res 114(B8):B08309. doi:10.1029/2008JB006101

Olson AH, Aspel RJ (1982) Finite faults and inverse theory with applications to the 1979 Imperial Valley earthquake. Bull Seismol Soc Am 72(6A):1969–2001

Roten D, Miyake H, Koketsu K (2012) A Rayleigh wave back-projection method applied to the 2011 Tohoku earthquake. Geophys Res Lett 39(2):L02302. doi:10.1029/2011GL050183

Satoh T, Kawase H, Sato T (1997) Statistical spectral model of earthquakes in the eastern Tohoku district, Japan, based on the surface and borehole records observed in Sendai. Bull Seismol Soc Am 87(2):446–462

Sekiguchi H, Irikura K, Iwata T (2000) Fault geometry at the rupture termination of the 1995 Hyogo-ken Nanbu earthquake. Bull Seismol Soc Am 90(1):117–133

Sekiguchi H, Irikura K, Iwata T (2002) Source inversion for estimating the continuous slip distribution on a fault—introduction of Green's functions convolved with a correction function to give moving dislocation effects in subfaults. Geophys J Int 150(2):377–391

Shao G, Xi L, Ji C, Maeda T (2011) Focal mechanism and slip history of 2011 Mw9.1 off the Pacific coast of Tohoku earthquake, constrained with teleseismic body and surface waves. Earth Planets Space 63(7):559–564

Somerville PG, Irikura K, Graves R, Sawada S, Wald D, Abrahamson N, Iwasaki Y, Kagawa T, Smith N, Kowada A (1999) Characterizing crustal earthquake slip models for the prediction of strong ground motion. Seismol Res Lett 70(1):59–80

Suzuki W (2008) Estimation of broadband source process based on strong motion modeling. Ph.D Thesis, Kyoto University, 130 pp

Suzuki W, Iwata T (2005) Source characteristics of interplate earthquakes in northeast Japan inferred from the analysis of broadband strong-motion records. Eos Trans AGU 86(52), Fall Meet. Suppl., Abstract S43A-1040

Suzuki W, Iwata T (2007) Source model of the 2005 Miyagi-oki, Japan, earthquake estimated from broadband strong motions. Earth Planets Space 59(11):1155–1171

Suzuki W, Aoi S, Sekiguchi H, Kunugi T (2011) Rupture process of the 2011 Tohoku-Oki mega-thrust earthquake (M9.0) inverted from strong-motion data. Geophys Res Lett 38:L00G16. doi:10.1029/2011GL049136

Takiguchi M, Asano K, Iwata T (2011) The comparison of source models of repeating subduction-zone earthquakes estimated using broadband strong motion records –1982 and 2008 Ibaraki-ken-oki M7 earthquakes–. Zisin 2 (J Seismol Soc Japan) 63(4):223–242 (in Japanese with English abstract)

Wang D, Mori J (2011) Rupture process of the 2011 off the Pacific coast of Tohoku earthquake (Mw9.0) as imaged with back-projection of teleseismic P-waves. Earth Planets Space 63(7):603–607

Wessel P, Smith WHF (1998) New, improved version of generic mapping tools released. Eos Trans AGU 79(47):579

Yagi Y, Fukahata Y (2011a) Rupture process of the 2011 Tohoku-oki earthquake and absolute elastic strain release. Geophys Res Lett 38(19):L19307. doi:10.1029/2011GL048701

Yagi Y, Fukahata Y (2011b) Introduction of uncertainty of Green's function into waveform inversion for seismic source process. Geophys J Int 186(2):711–720

Yokota Y, Koketsu K, Fujii Y, Satake K, Sakai S, Shinohara M, Kanazawa T (2011) Joint inversion of strong motion, teleseismic, geodetic, and tsunami datasets for the rupture process of the 2011 Tohoku earthquake. Geophys Res Lett 38:L00G21. doi:10.1029/2011GL050098

Yoshida S, Koketsu K, Shibazaki B, Sagiya T, Kato T, Yoshida Y (1996) Joint inversion of the near- and far-field waveforms and geodetic data for the rupture process of the 1995 Kobe earthquake. J Phys Earth 44(5):437–454

Yoshida K, Miyakoshi K, Irikura K (2011a) Source process of the 2011 off the Pacific coast of Tohoku earthquake inferred from waveform inversion with long-period strong-motion records. Earth Planets Space 63(7):577–582

Yoshida Y, Ueno H, Muto D, Aoki S (2011b) Source process of the 2011 Off the Pacific coast of Tohoku earthquake with the combination of teleseismic and strong motion data. Earth Planets Space 63(7):565–569

Yue H, Lay T (2011) Inversion of high-rate (1 sps) GPS data for rupture process of the 11 March 2011 Tohoku earthquake (Mw9.1). Geophys Res Lett 38:L00G09. doi:10.1029/2011GL048700

Zhang H, Ge Z, Ding L (2011) Three sub-events composing the 2011 off the Pacific coast of Tohoku earthquake (Mw9.0) inferred from rupture imaging by back-projecting teleseismic P waves. Earth Planets Space 63(7):595–598

Zhao D, Hunag Z, Umino N, Hasegawa A, Kanamori H (2011) Structural heterogeneity in the megathrust zone and mechanism of the 2011 Tohoku-oki Earthquake (Mw9.0). Geophys Res Lett 38(17):L17308. doi:10.1029/2011GL048408